



HAL
open science

On the electronic properties and catalytic activity of MoS₂-C₃N₄ materials prepared by one-pot reaction

D. Ryaboshapka, P. Bargiela, L. Piccolo, P. Afanasiev

► **To cite this version:**

D. Ryaboshapka, P. Bargiela, L. Piccolo, P. Afanasiev. On the electronic properties and catalytic activity of MoS₂-C₃N₄ materials prepared by one-pot reaction. *International Journal of Hydrogen Energy*, 2022, 47 (80), pp.34012-34024. 10.1016/j.ijhydene.2022.08.034 . hal-03837826

HAL Id: hal-03837826

<https://hal.science/hal-03837826>

Submitted on 9 Nov 2022

HAL is a multi-disciplinary open access archive for the deposit and dissemination of scientific research documents, whether they are published or not. The documents may come from teaching and research institutions in France or abroad, or from public or private research centers.

L'archive ouverte pluridisciplinaire **HAL**, est destinée au dépôt et à la diffusion de documents scientifiques de niveau recherche, publiés ou non, émanant des établissements d'enseignement et de recherche français ou étrangers, des laboratoires publics ou privés.

On the electronic properties and catalytic activity of MoS₂-C₃N₄ materials prepared by one-pot reaction.

Daria Ryaboshapka*, Pascal Bargiela, Laurent Piccolo, Pavel Afanasiev*

Univ Lyon, Univ. Claude Bernard Lyon 1, CNRS, UMR5256, IRCELYON, F-69626, Villeurbanne, France.

Abstract

MoS₂-C₃N₄ composite materials with Mo content from 0.3 to 9 wt.% have been prepared by means of one-pot synthesis from ammonium thiomolybdate (NH₄)₂MoS₄ and urea. The solids were characterized by several physical techniques and tested in the thiophene hydrodesulfurization model reaction (HDS) and photocatalytic hydrogen evolution reaction (PHER). Transmission electron microscopy (TEM) and X-ray absorption spectroscopy (XAS) show that, even at the smallest Mo contents, the solids contain individual MoS₂ and C₃N₄ phases. As attested by powder X-ray diffraction (XRD), addition of thiomolybdate salt impacts the properties of obtained C₃N₄, probably at the growth stage, leading to more disordered carbon nitride phase. However, the materials demonstrate electronic properties close to superposition of two separate MoS₂ and C₃N₄ phases, as follows from the results of UV-visible diffuse reflectance spectroscopy (UV-vis DRS) combined with Ultraviolet and X-ray photoelectron spectroscopies (UPS, XPS). The band alignment diagram constructed from the UV-vis DRS, XPS and UPS data is of staggered type, with valence band of MoS₂ higher than that of C₃N₄. Composite materials have high thiophene HDS activity, increasing in step with the Mo content, which proves fine dispersion of MoS₂ phase and good availability of MoS₂ edges to the reactants. By contrast, PHER activity first increases with the Mo loading and then it decreases, reflecting the competition between the ability of MoS₂ to promote associative desorption of hydrogen and its role as a charge carriers recombination sink.

Keywords: carbon nitride; molybdenum sulfide; hydrodesulfurization; photocatalytic water splitting; band alignment, UPS

Introduction

Carbon nitride C₃N₄ is a widely studied 2D material for many emerging applications.¹ It is used as a heterogeneous catalyst,^{2,3} a catalytic support stabilizing single atoms,^{4,5} a reactive template for nanomaterials synthesis^{6,7} and as a semiconductor in photocatalysis.^{8,9} C₃N₄

possesses advantageous properties as a semiconductor such as ability to absorb light in UV and visible regions, suitable position of conduction and valence bands (CB and VB) for redox reactions, low cost, low environmental impact and thermal/chemical stability.^{10,11} However, application of pure C₃N₄ in photocatalysis is limited by low mobility and fast recombination of charge carriers and low absorption in visible region.^{12,13,14,15} By this reason, C₃N₄ is usually applied in the composite materials containing versatile co-catalysts, including metallic nanoparticles,¹⁶ metal oxides,¹⁷ sulfides,¹⁸ or ferrites.¹⁹

Molybdenum sulfide MoS₂ was previously studied as a co-catalyst for C₃N₄ in the photocatalytic reactions.^{20,21} MoS₂ is a semiconductor, but unlike C₃N₄, it mostly absorbs light in the visible region. At the same time MoS₂ is a well-known catalyst because the edges of MoS₂ slabs provide catalytic sites for the reactions involving hydrogen, such as hydrodesulfurization²² or electrochemical hydrogen evolution.²³ Since both MoS₂ and C₃N₄ possess layered (2D) structures, formation of interface junction between these materials was considered.²⁴ The heterojunction between MoS₂ and C₃N₄ was reported to decrease electron-hole recombination with electrons migrating to the surface of MoS₂ particles and reacting with adsorbed protons.^{25,26} In some works, it is suggested that due to interactions between MoS₂ and C₃N₄ the electronic properties are modified and the band gap of MoS₂-C₃N₄ becomes lower than that of pure C₃N₄, leading to a higher absorption in the visible region and therefore a higher catalytic activity.^{25,26} In other works, however, unchanged bandgap value is reported.^{15,27} Therefore, the nature of the electronic interaction and the role of MoS₂ in the increased catalytic activity of MoS₂-C₃N₄ still remain a matter of controversy.

In this work we prepared via one-pot route a series of composite MoS₂-C₃N₄ catalysts and studied their catalytic performance in HDS of thiophene and photocatalytic hydrogen evolution. Physical characterizations have been carried out to explain the trends of catalytic properties, unravel the interactions between MoS₂ and C₃N₄, and clarify band alignment in these composite materials.

Experimental

Preparation of the MoS₂-C₃N₄ catalysts

The synthesis procedure is similar to one described earlier in Ref.²⁵. In brief, 5 g of urea, 5 g of thiourea were thoroughly mixed with different amounts of (NH₄)₂MoS₄ (10, 30, 100, 300 mg) in a Pyrex tube reactor. The reactor was placed in an oven and heated in Ar atmosphere to 550 °C for 2 h (heating rate 5 °C/min). Approximately 1.2 g of the solid was obtained in all cases. To

activate the samples prior to the catalytic tests, sulfidation was performed in a Pyrex reactor in 15 vol.% H₂S/H₂ flow at 350 °C for 1 h, with a heating rate 5 °C min⁻¹. The samples containing 0.3, 0.9, 3.1 and 9.2 wt.% Mo were prepared. The samples are designated according to the molybdenum loading. Thus, 0.3Mo-C₃N₄ represents the solid containing 0.3 wt.% Mo. Bare C₃N₄ reference was obtained using the same procedure without addition of (NH₄)₂MoS₄. Reference bulk MoS₂ was obtained by decomposing (NH₄)₂MoS₄ in H₂/H₂S flow at 750 °C. High sulfidation temperature was applied in this case in order to obtain highly crystalline materials with extended slabs and therefore to minimize the effects of air exposure.

Hydrodesulfurization (HDS) of thiophene

Thiophene HDS was studied in the gas phase at the atmospheric pressure. After sulfidation, 250 mg of the sample was placed into a Pyrex microreactor and heated up to 320 °C at 5 °C min⁻¹ rate, under 50 ml min⁻¹ H₂ flow, saturated with thiophene at 0 °C. The reaction products were analyzed by gas chromatography on an Agilent 7820A device. More experimental details are reported in Ref.²⁸

Photocatalytic hydrogen production (PHER)

PHER was studied in a liquid slurry, using methanol as a sacrificial agent. In a typical procedure, 20 mg of the catalyst were dispersed in 30 ml of methanol in an ultrasonic bath. The obtained suspension was then transferred into the reaction cell. Prior to reaction the suspension was stirred for 10 min and simultaneously Ar was purged through the cell. An HPK lamp was used as a photon source. The products were analyzed by Agilent 3000 A micro gas chromatograph. More experimental details are reported in Ref.²⁹.

Physico-chemical characterizations

All characterizations were performed for samples taken after sulfidation in H₂S/H₂, unless stated otherwise.

Textural properties of the C₃N₄ and Mo-C₃N₄ samples were investigated by N₂ adsorption-desorption volumetry using Micrometrics ASAP 2010 device. Prior to measurements the samples were outgassed under secondary vacuum at 350°C for 2 h. FTIR spectra were recorded on an Agilent Cary 630 spectrometer, in the wavenumber range from 650 to 4000 cm⁻¹. Phase composition was studied by powder X-ray diffraction (XRD) on a Bruker D8 Advance A25 diffractometer with CuK α emission. The crystalline phases were identified by comparison with the JCPDS standards database. The quantities of light elements were determined by means of CHNS analysis on a Thermo Fisher Flash 2000 device. The amount of Mo in the Mo-C₃N₄ samples

was quantified by inductively coupled plasma-optical emission spectroscopy (ICP-OES, Activa instrument from Horiba Jobin Yvon). Transmission Electron Microscopy (TEM) photographs were obtained on a JEOL 2010 instrument operating at 200 kV. Digital Micrograph Gatan program package was applied for analysis of TEM images.

The coordination environment of Mo in Mo-C₃N₄ samples was studied *ex-situ* by X-ray absorption spectroscopy (XAS) at the ROCK beamline of SOLEIL synchrotron. Prior to measurements the powders were pressed into 6 mm diameter tablets and put on the sample holder between two Kapton layers. The spectra were recorded at the Mo K edge using a Si(220) channel-cut monochromator. The preliminary procedures such as merging of the spectra and alignment were performed with the ATHENA software.³⁰ Extended X-ray Absorption Fine Structure (EXAFS) spectra were fitted with the VIPER program³¹, in the *k* and *R* spaces (Im+Module mode).

UV-vis diffuse reflectance spectroscopy (UV-vis DRS) was performed on a Perkin Elmer Lambda 35 device. BaSO₄ was used as a reference compound with 100% reflectance. 20 mg of each sample were thoroughly mixed with 1 g of BaSO₄ and ground into powder; then it was placed into the UV-vis cell. The spectra were recorded in the reflectance mode, in the wavelength range from 1000 to 200 nm.

X-ray photoelectron spectroscopy (XPS) was carried out on a Kratos Axis Ultra DLD spectrometer, using as X-ray source the monochromatic Al K α radiation (1486.6 eV), operating at 180 W, 12 kV, 15 mA. Prior to the experiment the samples were crushed into powder and pressed onto a conductive carbon tape under argon atmosphere. The survey spectra were registered in the interval 1200–0 eV with a pass energy of 160 eV. High-resolution spectra, pass energy of 40 eV, were obtained for O 1s, N 1s, Mo 3d+S 2s, C 1s, S 2p and valence band regions. The spectra were treated with CasaXPS software. For the spectra alignment, the C 1s photoemission peak of adventitious carbon was located at 284.8 eV.

Ultraviolet photoelectron spectroscopy (UPS) analyses were conducted in an integrated ultrahigh vacuum system, connected to an A Axis Ultra DLD spectrometer (Kratos Analytical). UPS spectra were obtained with a He lamp using resonance line He I ($h\nu = 21.2$ eV). The samples for UPS measurements were prepared by sticking onto a conducting carbon tape or by other techniques, to minimize the charging effects, as described in Ref.³². In brief, the powders were ultrasonically dispersed in heptane or methanol. Then, several drops were deposited on the conducting FTO (fluorine-doped SnO₂) substrate.

3. Results and discussion

3.1. Properties of the composite materials.

Routine physical characterizations (XRD, N₂ adsorption, chemical analysis) allowed us to follow the influence of the reaction mixture composition on the properties of the resulted composite materials such as specific surface area, chemical composition and crystallinity.

Specific surface area values (Table 1) slightly increase with the Mo loading, suggesting that C₃N₄ becomes more disordered upon the addition of thiomolybdate. The isotherms shape (Fig. 1a) are characteristic of materials containing macropores and large mesopores. Pore size distribution has a maximum at 27 nm (Fig. 1b).

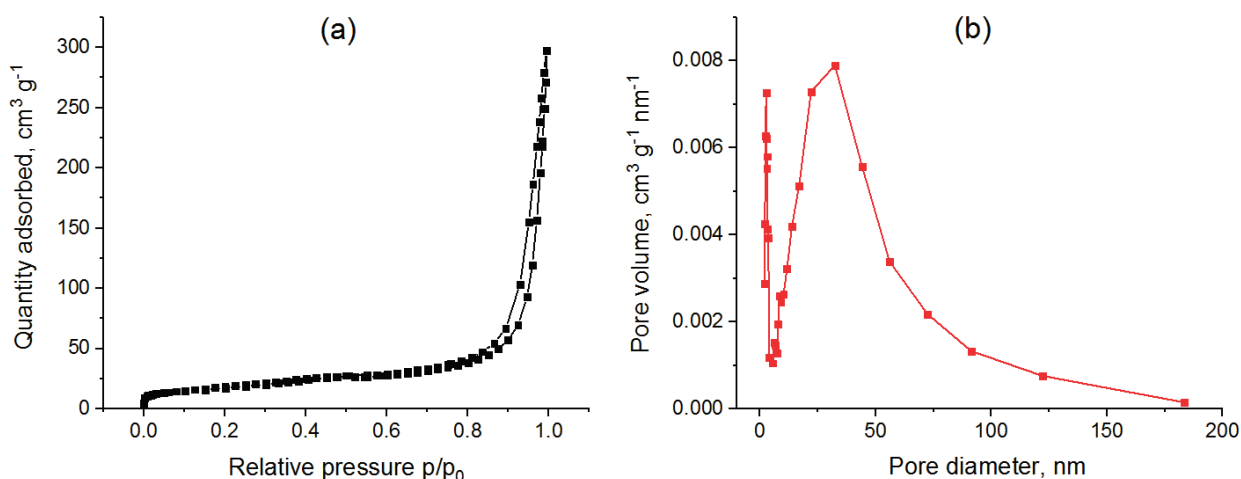


Figure 1. (a) N₂ adsorption-desorption isotherm and (b) BJH pore size distribution, as exemplified for the 0.3Mo-C₃N₄ sample.

The results of elemental analysis are shown in Table 1. The absence of sulfur in the bare C₃N₄ (prepared using thiourea precursor) suggests that all sulfur has left during the preparation, in the form of H₂S, CS₂ or other volatile compounds.¹¹ Therefore, in all the Mo-containing samples, sulfur probably belongs to some MoS_x species. The stoichiometric C₃N₄ should contain 61 wt.% of nitrogen and 39 wt.% of carbon, while in our samples there is always an excess of nitrogen (Table 1). Positive values of mass balance Δ for bare C₃N₄ and 0.3Mo-C₃N₄ reflect on the technique accuracy. With the increase of Mo content, the amounts of both C and N decrease, but the C/N atomic ratio increases slightly, indicating that more nitrogen leaves the system. Oxygen was not explicitly analyzed, but its amount can be estimated from the mass balance Δ . While the amount of oxygen seems low in the bare C₃N₄, 0.3Mo-C₃N₄ and 0.9Mo-C₃N₄ samples, the values of negative Δ are obviously beyond the error margin for the 3.1Mo-C₃N₄ ($\Delta = -4.5\%$) and 9.2Mo-C₃N₄. ($\Delta = -9.3\%$). That amount of oxygen cannot be bound to molybdenum (vide infra for characterizations of molybdenum coordination by XAS), so it should be present in the carbon nitride, where it probably compensates the decreasing amount of nitrogen. Apparently, the

majority of oxygen comes from the urea used for preparation. It was suggested in our previous paper that Mo species might act as a catalyst for decomposition of carbon nitride.⁷ Here, thiomolybdate species seem to modify the reaction pathway and influence final composition of the resulting C₃N₄.

To check whether there is a structural change accompanying variations of the chemical composition, the materials were studied by means of Fourier transform infrared spectroscopy (FTIR). FTIR spectra of 9.2Mo-C₃N₄ sample and C₃N₄ are presented in Figure S1. The band at 810 cm⁻¹ is attributed to breathing vibration of tri-s-triazine units in C₃N₄,^{33,34} while the band centered around 889 cm⁻¹ is ascribed to deformation mode of N-H bond.³⁵ The abundant peaks in the 1200 – 1700 cm⁻¹ region are characteristic of stretching vibrations of C=N and C-N bonds.³⁵ The peaks in the region 3000 – 3500 cm⁻¹ might correspond to the stretching vibrations of N-H bonds and/or to the vibrations of adsorbed H₂O molecules.^{34,35} With addition of 9.2 wt.% of Mo no significant changes in the spectrum occur, but only a small decrease of all bands intensity. Therefore, molybdenum and/or oxygenated species present in the structure are smeared in frequency or have low absorption intensity, so that they do not give rise to any new distinct features.

Table 1 Results of chemical analysis and surface area measurements

Sample	Mo, wt. %	N, wt. %	C, wt. %	H, wt. %	S, wt. %	C/N ^a	Δ,% ^b	S _{BET} , m ² /g
C ₃ N ₄	0	67.8	34.2	1.4	0.0	0.58	3.4	56
0.3Mo-C ₃ N ₄	0.26	65.8	33.8	1.5	0.2	0.60	1.6	67
0.9Mo-C ₃ N ₄	0.80	60.9	33.0	1.5	0.5	0.62	-3.2	66
3.1Mo-C ₃ N ₄	2.82	57.4	31.7	1.4	1.9	0.66	-4.5	75
9.2Mo-C ₃ N ₄	8.39	47.4	27.4	1.2	5.5	0.67	-9.3	91
Ideal C ₃ N ₄	0	61.0	39.0	0.0	0.0	0.74	0	-

^a atomic ratio, ^b sum of all percentages – 100%.

The results of powder XRD confirm the influence of thiomolybdate addition on the properties of carbon nitride. The XRD pattern of C₃N₄ shows typical features at 27.6°, 21.5° and 12.7°, corresponding to (002), (100), (001) planes, respectively (Fig. 2). With the increase of Mo loading the intensity of all C₃N₄ reflections decreases, suggesting increased disorder of the structure (Fig. 2). At the same time no shift of XRD lines occurs, attesting that the same C₃N₄ structure is preserved. At the Mo loading 3.1 wt. % and higher, broad reflections of MoS₂ phase appear at 33 ° (100) and 59 ° (110). Remarkably, there is no strong (002) line expected at 14.5° of the stable 2H-MoS₂ phase (JCPDS card no.75-1539). Instead, a small ill-resolved peak located at ~9.7 ° (9.1 Å) appears, which is often attributed to the (001) line of metallic 1T-MoS₂ phase.^{36,37}

³⁸ However, an increase of the (002) distance does not prove alone the formation of the 1T phase, which requires convergence of several characterizations (UV-vis DRS, Raman, TEM).

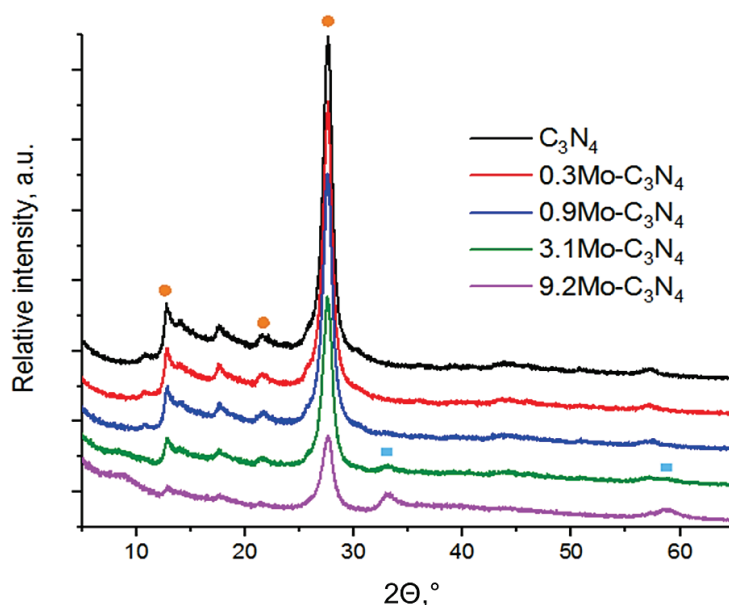
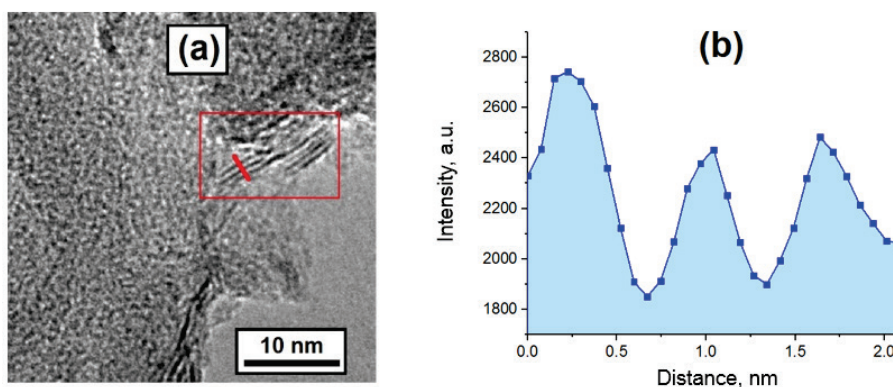


Figure 2 XRD patterns of C_3N_4 and sulfided samples; orange circles indicate reflexes of C_3N_4 phase (01-087-1526) and blue squares – reflexes of 2H- MoS_2 phase (00-006-0097)

3.2. Chemical state of molybdenum in the solids

For the high-loaded samples the presence of MoS_2 phase is evidenced by the XRD patterns (Fig. 2). However, the overall chemical state of molybdenum, and in particular in the low-loaded samples remains unclear and should be clarified. Before starting the preparations, we checked that a homogeneous solution of thiomolybdate in molten urea/thiourea was formed upon heating of the reaction mixtures. We assumed that if molybdenum was spread homogeneously in the solution, then for low loadings we might have obtained the materials with ultradispersed or single-atomic Mo species, possibly coordinated by sulfur and/or by nitrogen of the C_3N_4 cavities. For these reasons we proceeded with TEM, XAS and XPS characterizations.



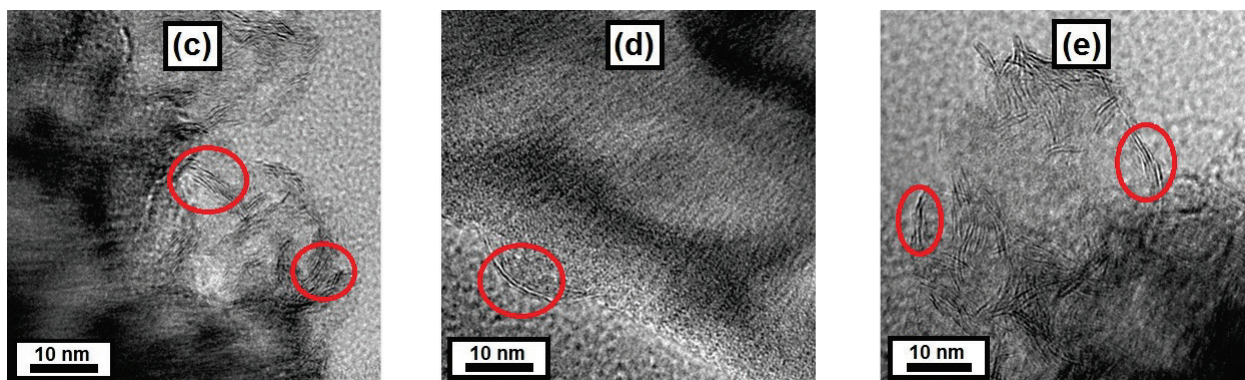


Figure 3 (a) TEM image of 9.2 Mo-C₃N₄ (b) intensity distribution along the red line, TEM images of (c) 0.9Mo-C₃N₄, (d) 3.1Mo-C₃N₄, (e) 9.2Mo-C₃N₄

High resolution TEM revealed the presence of MoS₂ slabs in all the samples except for 0.3Mo-C₃N₄, though in the low-loaded 0.9Mo-C₃N₄ sample they are few and rather hard to find. In the samples with higher loadings the MoS₂ slabs are expectedly more abundant (Fig. 3). Notably, at the nanoscale, the slabs are not spread uniformly over C₃N₄, but concentrated in some zones, whereas extended zones of carbon nitride are free from sulfide. In agreement with the XRD results, the distance between the MoS₂ layers in TEM images is around 0.9 nm, i.e. considerably increased if compared with the interplane distance (002) for 2H-MoS₂ (0.62 nm), indicating the increased disorder.

Core-level XPS spectra have been acquired for bare C₃N₄, reference MoS₂ and 9.2Mo-C₃N₄ samples. For bare C₃N₄, deconvolution of C1s spectrum gives three main contributions (Fig. S2b): the signal of adventitious carbon at 284.8 eV; the major signal at 288.1 eV corresponding to C – N bonds in triazine units (C surrounded by three N atoms) and the contribution at 289.4 eV that might be assigned to C – (N₄).³⁹ As for N1s spectrum (Fig. S2c), three major contributions are observed: 398.6 eV, 399.7 eV and 401 eV. The first one corresponds to sp² hybridized N in N-C=N, the second – to N bonded with three carbon atoms (N-(C₃)), the third one – to nitrogen in NH₂ group.^{40,41} The peak around 404.2 eV is probably due to a π-excitation in C₃N₄, similar to that observed for melamine.⁴² For the reference MoS₂, in the S 2p spectrum only one doublet is observed at 162.9 and 161.7 eV, characteristic of S²⁻ (Fig. S3c).⁴³ Deconvolution of the Mo 3d signal gives one doublet at 232 eV and at 228.8 eV, which is typical for sulfided Mo (IV) in MoS₂ (Fig. S3b).⁴³

For the 9.2Mo-C₃N₄ sample, the C1s and N1s spectra are similar to those of bare C₃N₄ (Fig. 4c and 4d). The only difference is the appearance of a minor peak around 290.5 eV in the C1s spectrum, corresponding to oxygenated species such as carboxylate groups, coming from urea precursor.⁴⁴ The presence of oxygenated groups agrees with the results of chemical analysis that suggest the presence of oxygen in the highly-loaded samples. In the Mo 3d spectrum, sulfidic

Mo(IV) is observed at the same BE as in the MoS₂ reference (Fig. 4a). The edges of the MoS₂ slabs are partially oxidized under air, so the contribution of Mo(V) (5/2 at 231 eV and 3/2 at 234.2 eV) appears, which is an intermediate species in MoS₂ oxidation in air.⁴⁵ This attribution is also supported by the presence of minor amount of oxidized sulfur in the S2p spectrum (Fig. 4b). The doublet of S²⁻ species (161.5 and 162.8 eV) is the major sulfur species in MoS₂. According to the XPS results, the composite material behaves as a mechanic mixture of MoS₂ and C₃N₄, without any noticeable shifts in the binding energies in the main spectral lines of composing elements.

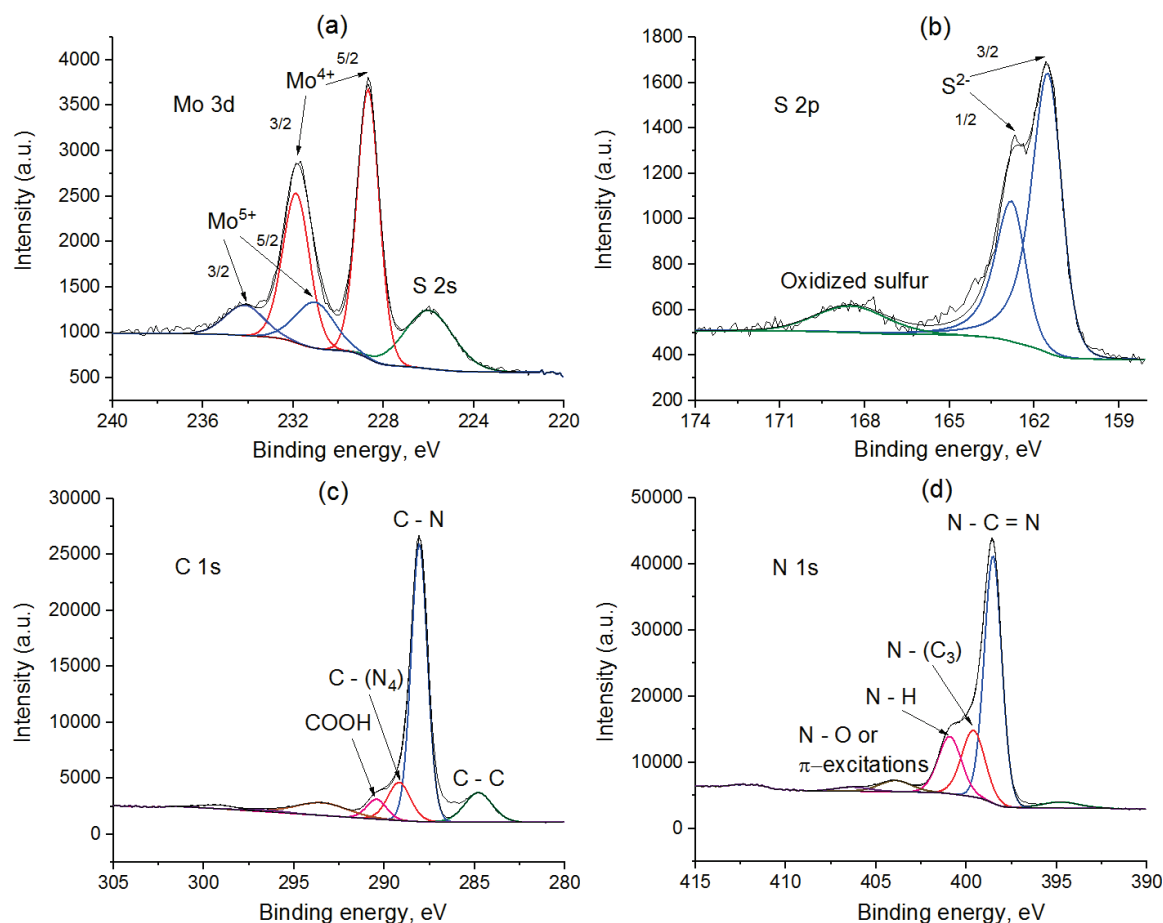


Figure 4 XPS spectra of 9.2Mo-C₃N₄ (a) Mo 3d (b) S 2p (c) N1s (d) C1s

While TEM study evidences the formation of MoS₂ slabs, it remains unclear whether all molybdenum is present as sulfide slabs, or it is distributed between MoS₂ and other forms not detectable by TEM. To answer this question, we proceeded with the Mo K edge XAS characterization that provides information about coordination and oxidation state of all Mo species contained in the sample. We recorded *ex-situ* spectra of the samples before and after sulfidation. The XANES spectra (Fig. 5a) do not demonstrate significant differences with increasing Mo loading and resemble that of reference MoS₂ compound (a small feature resembling a pre-edge in the spectra of low-loaded samples is an artifact). The shapes of EXAFS spectra are also very similar (Fig. 5b). The experimental spectra and the corresponding fits in R and k spaces are

presented in Figures S4 – S7. To obtain a good fit, all spectra require S and Mo neighbors at 2.40 and 3.13 Å, respectively (Table 2), typical for bulk MoS₂. The coordination numbers (CN) of S and Mo are slightly different from the theory values (6 for both Mo and S) for the bulk sulfide. In all samples, five sulfur atoms are required to fit the sulfur environment. The CN of Mo varies slightly with Mo loading, from 4 in the 0.3Mo-C₃N₄ to 5 in the 9.2Mo-C₃N₄. The obtained CNs of Mo neighbors suggest a slight increase of the MoS₂ slabs dispersion from high-loaded 9.2Mo-C₃N₄ to low-loaded samples. Note that even for the lowest loading of Mo (0.3 wt.%) the coordination is close to that of bulk MoS₂. A small contribution of oxygen as a short Mo=O bond (1.72 Å) improves the goodness of the fit in case of low-loaded samples, suggesting that the slabs edges were slightly oxidized because of short exposure to air. No nitrogen or carbon atoms at their characteristic distances are present in Mo coordination environment, suggesting that incorporation of Mo into carbon nitride network did not occur and all Mo remains in form of MoS₂. There is no significant difference between the spectra of samples taken before and after sulfidation (Fig. 5c) meaning that MoS₂ was formed already during the preparation in Ar, whereas the role of sulfidation is only to activate the slabs edges.

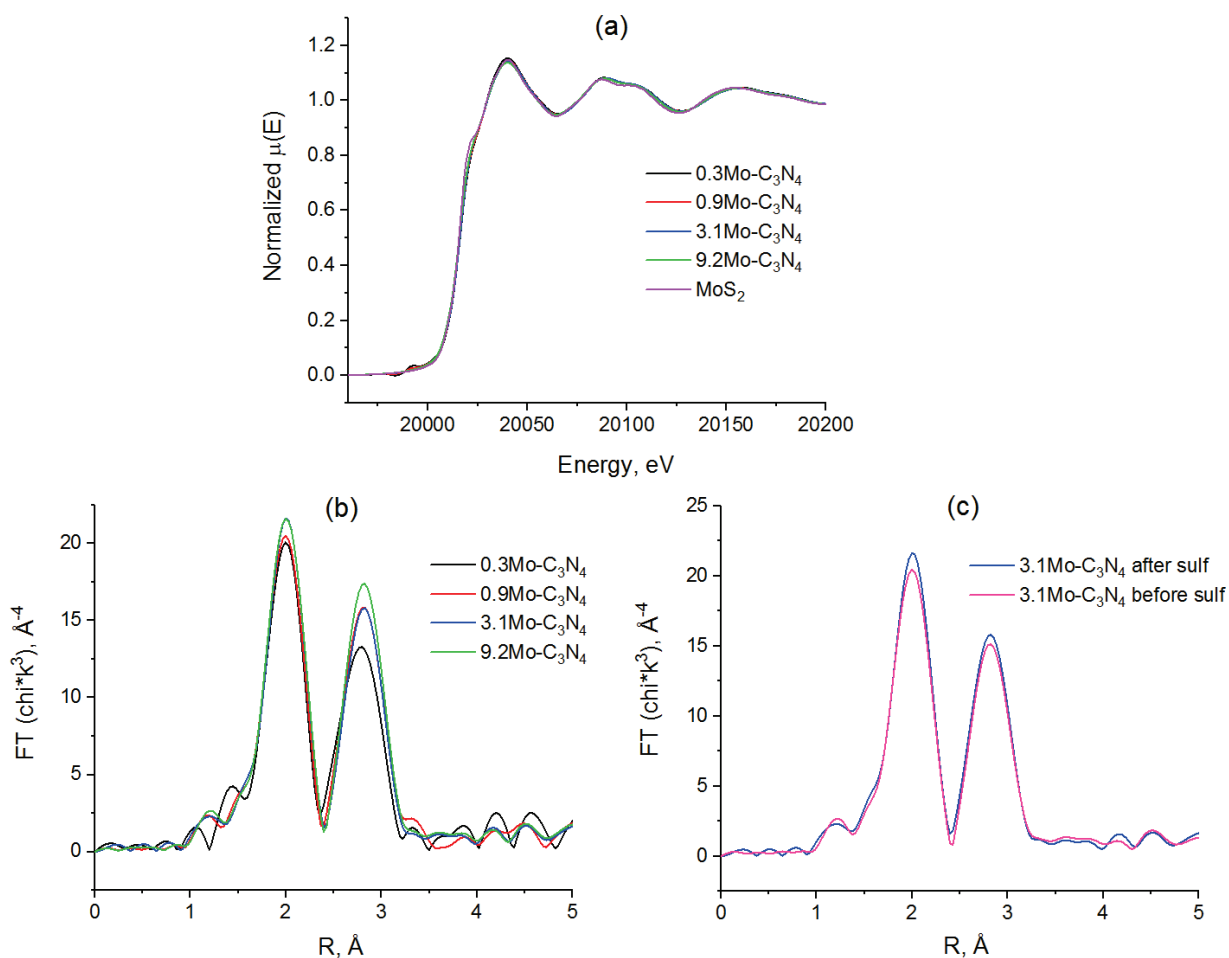


Figure 5 (a) XANES spectra of sulfided samples and of MoS₂ reference (b) EXAFS spectra in R-space for sulfided samples (c) EXAFS spectra in R-space before and after sulfidation.

Table 2 EXAFS fitting results in R-space for the sulfided samples

Scatterer atom	CN ^a	R (Å) ^b	σ^2 (Å ²) ^c	ΔE_0 (eV) ^d
0.3Mo-C₃N₄, R = 0.09				
O	0.5(2)	1.72(1)	0.0037(9)	-1(1)
S	5.0(2)	2.40(1)	0.0039(9)	2(1)
Mo	4.0(2)	3.13(1)	0.0048(9)	-5(1)
0.9Mo-C₃N₄, R = 0.07				
O	0.6(2)	1.72(1)	0.0068(2)	0(1)
S	5.0(2)	2.40(1)	0.0036(9)	2(1)
Mo	3.8(2)	3.14(1)	0.0041(9)	-1(1)
3.1Mo-C₃N₄, R = 0.04				
O	0.4(2)	1.74(1)	0.0057(9)	0(1)
S	5.0(2)	2.40(1)	0.0033(9)	3(1)
Mo	4.2(2)	3.14(1)	0.0045(9)	0(1)
9.2Mo-C₃N₄, R = 0.05				
S	5.0(2)	2.40(1)	0.0032(9)	2(1)
Mo	4.8(2)	3.14(1)	0.0047(9)	0(1)

^a Coordination number, assuming $S_0^2 = 1.0$; ^b distance to the neighboring atom; ^c distance variance; ^d energy variance (free variable between -5 and 5 eV)

It follows from the TEM, XPS and XAS characterizations that MoS₂ is the predominant species in our samples already at the lowest Mo loadings. Notably, ammonium thiomolybdate is well soluble in molten urea, forming a dark-red solution at the temperatures below 200 °C. It appears however that reaction at higher temperatures does not allow incorporation of any considerable amount of single-atomic Mo species into the carbon nitride framework (as it happens for many divalent and trivalent cations of metals^{46,47}), but leads to quantitative precipitation of MoS₂. Perhaps, unlike the cationic species that tend to be coordinated with nitrogen lone electronic pairs of the carbon nitride structure, the MoS₄²⁻ anion has no affinity towards nitrogen in the C₃N₄ cavities. By this reason MoS₄²⁻ anions condense in the melt at higher temperatures and finally decompose to MoS₂ phase.

3.3. Catalytic properties

Thiophene hydrodesulfurization (HDS) model catalytic test was applied to access sulfide dispersion, chemical reactivity of the edges and availability of sulfide slabs within the material to the reactant molecules.

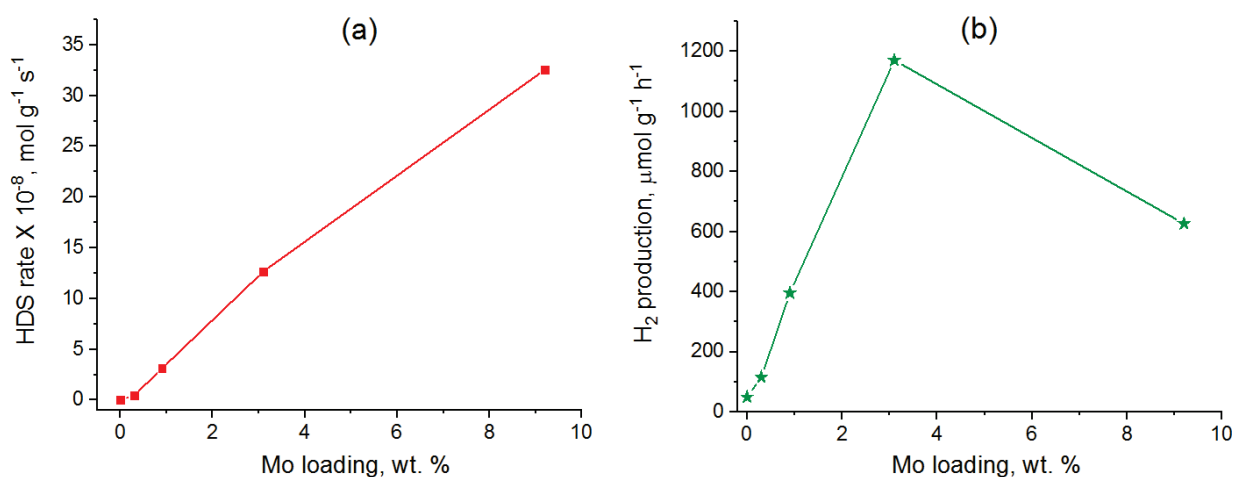


Figure 6 Catalytic properties vs Mo loading: (a) steady state thiophene HDS rates measured at 320 °C; (b) rates of photocatalytic hydrogen production in methanol slurry.

The catalysts demonstrated considerable activity in thiophene HDS, steady state rates measured at 320 °C being: 5, 31, 127 and 325 $\text{nmol g}^{-1} \text{s}^{-1}$ for 0.3, 0.9, 3.1 and 9.2Mo-C₃N₄, respectively. The HDS rates increase almost linearly with the Mo loading (Fig. 6a). 9.2Mo-C₃N₄ does not follow the linear trend, the conversion for this sample is a bit lower than expected, possibly due to a bit lower dispersion of MoS₂ as observed by XAS. For the MoS₂/Al₂O₃ benchmark reference, containing 10% wt. of Mo, the mass specific HDS activity measured in the same conditions is in the range between 300 and 360 $\text{nmol g}^{-1} \text{s}^{-1}$.²⁸ Therefore, MoS₂-C₃N₄ composites as heterogeneous HDS catalysts behave similarly to highly divided supported molybdenum sulfide, containing several – nm MoS₂ slabs, finely dispersed at the surface of support and available to the gaseous reactants.

The selectivity distributions show similar trends for all samples and resemble those of bulk and supported MoS₂ catalysts (Fig. S8). The main products are butenes, low amounts of butane are observed, as well as methane and ethane (1% for 0.9Mo-C₃N₄ and 9.2Mo-C₃N₄, 6% for 3.1Mo-C₃N₄), appearing due to partial oxidation of MoS₂ in air. However, in the low-loaded catalyst the detection of reaction products becomes less reliable due to low conversion (0.1 %). Therefore, with respect of selectivity, the MoS₂-C₃N₄ composites also behave as conventional supported MoS₂ catalysts.

Photocatalytic activities of the samples were compared for photocatalytic hydrogen evolution reaction (PHER) in a methanol slurry (Fig. 6b). Bare carbon nitride demonstrates low activity with PHER rate of 49 $\mu\text{mol}\cdot\text{g}^{-1} \text{h}^{-1}$. For the composite materials, the hydrogen production rate increases linearly with the amount of molybdenum and reaches a maximum of 1170 $\mu\text{mol}\cdot\text{g}^{-1} \text{h}^{-1}$ for the catalyst containing 3.1 wt.% Mo; further increase of loading results in a drop of activity. The samples activated by sulfidation are almost twice more active than the initial ones (Fig. S9),

suggesting that activation of the slabs edges plays an important role in PHER rate. The rate of hydrogen production is similar to that of previously studied materials at comparable Mo loadings. Approximately recalculated with respect to photon flux of 300 mW Xe lamp applied in the previous studies, it corresponds to the value of 2.8 mmol. g⁻¹ h⁻¹, whereas previously reported PHER rate values for this type of materials lie in a wide range between 0.8 and 12 mmol. g⁻¹ h⁻¹.^{25,48,49,50,51} However, a straightforward comparison of PHER rates is not possible, as the spectral power distribution of the light source, the reaction system geometry, the loading of the slurry and the sacrificial agent are different from one work to another.

Unlike the thiophene HDS activity that increases almost linearly with Mo loading, an excess of MoS₂ co-catalyst has a negative impact on the PHER activity. This type of behavior was observed previously for MoS₂-C₃N₄ systems.²⁵ The loading at which maximum activity was attained, depends on the carbon nitride preparation (exfoliation) technique and on the MoS₂ dispersion, but always corresponds to relatively low loadings (few wt.% at highest). The effect is not limited by MoS₂-C₃N₄ systems. Earlier we observed this behavior for the MoS₂-TiO₂ systems: in the 0.5 – 2 wt.% loading range of MoS₂ PHER activity reached its maximum and started to drop after 2 wt.%.²⁹ The decrease of PHER activity at higher loadings was attributed to MoS₂ ability to facilitate electron-hole recombination or to non-productive light absorption (*vide infra*).

3.4. Interactions between C₃N₄ and MoS₂ and the reasons of improved PHER activity.

In order to better understand the variations of PHER activity due to the presence of MoS₂, we tried to access electronic interaction between the components in our catalysts. In the previous works two main explanations of better PHER activity were given: more efficient light absorption and better charge separation. In several previous studies the positive effect of MoS₂ was attributed to the improved light absorption. It was suggested that the band gap is decreased in the composite materials vs. individual carbon nitride which improves light absorption.^{25,26} Moreover, the light absorbed by MoS₂ in the visible region is supposed to be productively used by the composite material due to the formation of heterojunction.

To address the issues related to light absorption we proceeded with the UV-visible diffuse reflectance spectroscopy (UV-vis DRS). UV-vis DRS spectra for Mo-containing samples and C₃N₄ are shown in Fig. 7a (also see Fig. S10). For bare C₃N₄, the HOMO orbital mainly consists of N 2p orbital states, while the LUMO orbital is composed of C 2sp hybrid orbitals. Electronic transitions in C₃N₄ result in appearance of two broad peaks in UV region centered around 380 and 326 nm that might be assigned to π - π^* electronic transitions in conjugated ring systems.⁵² In the MoS₂ phase the conduction band (CB) and valence band (VB) are dominated by Mo 4d and S 3p

orbitals while contribution of Mo 4d is the largest for the CB. Addition of MoS₂ results in several changes in the spectra (Fig. 7a). The increase of intensity of MoS₂ peaks located at 480, 600 and 660 nm with Mo loading is observed, as expected. However, there is a remarkable increase of intensity of the peak around 320 nm without simultaneous increase of the one at 380 nm. This phenomenon was observed before: if more defects are introduced into C₃N₄, the intensity of this peak increased.⁵³ However, to our knowledge, it was never discussed in detail. In agreement with XRD, XPS and chemical analyses we conclude that with addition of Mo the C₃N₄ structure becomes more defective. We assume that this effect might be attributed to electronic transitions in the distorted C₃N₄ which has disordered structure due to the effect of Mo during the sample preparation. The UV-vis peaks of MoS₂ were extracted from the base line for better visibility (Fig. S10a). Within the method accuracy, positions of the MoS₂ peaks remain unchanged for all Mo loadings, which suggests that no significant modification of the electronic structure occurred due to the interaction between MoS₂ and C₃N₄.

The band gap estimated by means of Tauc equation for MoS₂ is 1.7 eV, which corresponds well to the experimental values^{54,55} for the direct band gap in bulk and few-layer MoS₂ (Fig. S12c). The band gap of carbon nitride in the bare C₃N₄ and Mo-C₃N₄ samples remains around 3 eV, the variations between the samples being lesser than 0.05 eV (Fig. 7b). Therefore, as opposed to several previous reports,^{25,26,56} we cannot conclude that the band gap of the composites is modified due to addition of Mo. The impact of MoS₂ related to the shift of the band gap can be ruled out.

It is worth emphasizing that for our PHER experiments we have intentionally chosen UV-light with a maximum at 370 nm and lying entirely in the carbon nitride light absorption zone (Fig. S18). As follows from Fig. 7a, light absorption increases slightly for the samples containing more molybdenum. However, the PHER catalytic activity increases at the same time by a factor of 30. Therefore, the band gap modification, would it occur or not, cannot possibly explain the observed variations of the catalytic activity. By the same token, MoS₂ cannot absorb light productively in our case. Indeed, the main variations of the UV-vis spectra due to addition of MoS₂ occur beyond the spectral region of our light source.

Formation of a heterojunction and better separation of photoinduced charge carriers are often evoked as main reasons of the improved PHER activity of the MoS₂-C₃N₄ catalysts.^{25,26,57} We compared the XPS, UPS and UV-vis DRS spectra of our materials in order to check the presence of significant interactions leading to modifications of electronic levels as well as to clarify the band alignment. The literature reports on the band alignment in the MoS₂-C₃N₄ solids are controversial. Basing on different physical measurements and on the theory calculations, both straddling^{25,58} and staggered^{26,59} alignments have been proposed. Moreover, the absolute values

of reported VB and CB energies differ by a value up to 1 eV between the different studies. In order to clarify the band alignment and to further investigate into the nature of the interaction occurring between MoS₂ and C₃N₄ we performed UPS and valence band XPS for bare C₃N₄, 9.2Mo-C₃N₄ and MoS₂ reference.

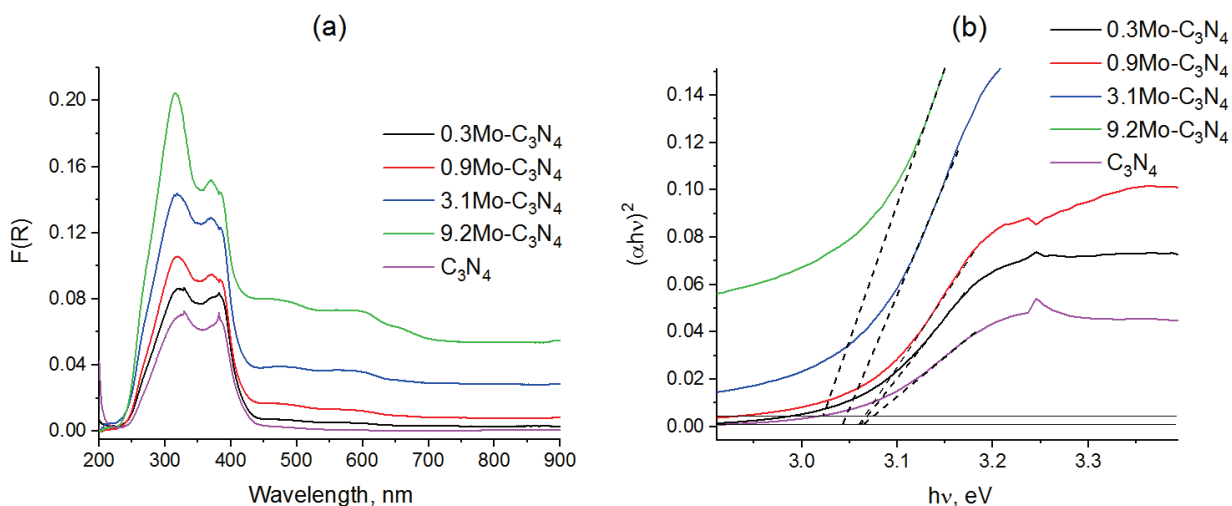


Figure 7 (a) UV-vis DRS spectra and (b) corresponding Tauc plots for sulfided Mo-C₃N₄ samples and C₃N₄ enlarged in C₃N₄ absorption region. Dashed lines represent linear dependences used to calculate band gaps, solid lines represent base lines.

The UPS spectrum of pure MoS₂ is presented in Fig S13a. The calculated work function (WF) value is about 5 eV, which is consistent with previous values for multilayered MoS₂ (4.98 eV).⁶⁰ The difference between Fermi level and valence band edge was estimated to be 0.93 eV. In a good agreement with UPS, analysis of XPS valence band provides a slightly lower value of 0.9 eV. From the UV-vis characterization the calculated band gap was 1.7 eV. Knowing these values we can estimate electron affinity (approx. 4.23 eV), which is close to values calculated by DFT and observed experimentally for several layer MoS₂ (4.3 eV).^{61,62} As for C₃N₄ reference we failed to obtain high-quality UPS spectra for any of the several sample preparation techniques that we tried. The reasons are discussed and the spectra are presented in the supplementary information (Fig. S15). In brief, low conductivity and closeness of valent zone to that of adventitious carbon make obstacle to obtaining clear cutoff value and/or reliable valence band edge. Therefore, we used combination of UPS for MoS₂ and XPS valent zone spectra to construct full band diagram (Fig. 8b). First, the UPS spectrum of MoS₂ was used to determine the absolute values of ionization energy, electron affinity and work function and then the XPS spectra allowed to place VB edge of C₃N₄ relative to MoS₂. Finally, the values of band gap from the UV-vis DRS spectra were used to locate the bottom of CB.

As follows from the XPS spectra of valent zone (Fig. 8a), the VB edge of C_3N_4 is by 2 eV lower as compared with MoS_2 . The spectrum of 9.2 $Mo-C_3N_4$ composite material is a superposition of two contributions from individual MoS_2 and C_3N_4 . Two inflexion points of the descending part of 9.2 $Mo-C_3N_4$ spectrum, at 2.8 and 0.7 eV, corresponding respectively to C_3N_4 and MoS_2 VB edges, are both shifted to lower BE by 0.1–0.2 eV, as compared with the spectra of individual components. This difference is at the limit of the method accuracy. Moreover, the same sign of shift for both components does not suggest transfer of electrons between them. Taking into account the optical band gap values we obtain the band alignment diagram (Fig. 8b), which is staggered, with the MoS_2 VB and CB levels located higher than those of C_3N_4 .

Several approaches exist to determine VB edge position from the photoemission spectra. Each one of them might become appropriate depending on the sample and the shape of the spectrum. The value of VB edge might be determined as: (i) the inflexion point of the descending VB spectrum; (ii) as a point of intersection of the slope with the baseline at low BE; (iii) as a point where the spectrum intensity increases by 1 – 3% above the baseline.⁶³ Physical rationale of each method depends on the nature of the analyzed system. Thus, if the slope of the descending part of density of states (DOS) at the VB edge is steep (has a step), then the observed XPS spectrum will be a convolution of this step with the instrumental linewidth profile, and the method (i) of the inflexion point should be used. Otherwise, if DOS at the VB edge decreases slowly, the methods (ii) and (iii) are more appropriate. The observed slope of VB edge of both C_3N_4 and MoS_2 is rather steep, as compared with the instrumental line width (about 1 eV as determined from calibration with clean Ag). Therefore, we assumed that the inflection point method (i) is the most appropriate for positioning VB in our system.

However, the VB positioned by other methods could be considered in combination with differently determined band gap values, in order to check the “stability” of the obtained band alignment diagram. Four different situations might be conceived, namely: (1) direct band gap of C_3N_4 combined with the VB determined from the inflection point (Fig. 8b); (2) direct band gap of C_3N_4 combined with the VB determined using the intersection point with the baseline (Fig. S14b); (3) indirect band gap of C_3N_4 and VB from the intersection point (Fig. S14a) and (4) indirect band gap of C_3N_4 and VB determined from the inflexion point. The last situation appears unphysical, because in this case the Fermi level should be higher than the LUMO of CB, leaving us only three options. It follows from the Fig. 8 and Fig. S14, that the conclusion on the staggered type of band alignment does not depend on the method of VB edge and band gap determination. Finally, even if the band gap of bulk MoS_2 obtained by theoretical calculations is used (1.3 eV), then the LUMO of MoS_2 will occupy the same position on the band alignment diagram as that of C_3N_4 , but not lower. Note that the use of direct vs. indirect band gap is a subtle problem for the nanomaterials at

stake, as neither the non-stoichiometric and distorted C_3N_4 nor the few-layer nanoscopic MoS_2 could be straightforwardly compared with the theory models. We consider that for the purposes of photocatalysis, the direct gap is more physically relevant as it corresponds to the onset of a non-negligible light absorption.

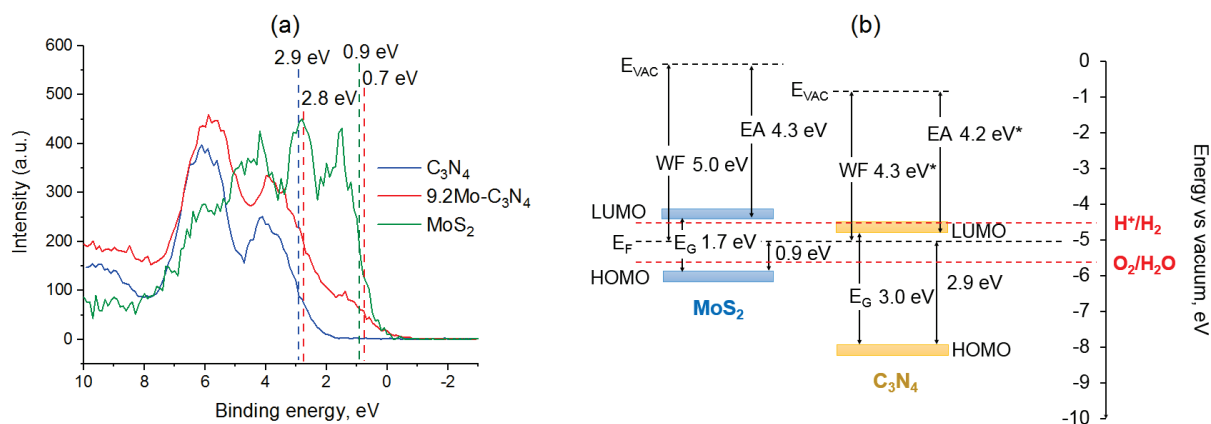


Figure 8 (a) XPS valence bands for C_3N_4 , MoS_2 and $9.2Mo-C_3N_4$, (b) Band alignment for MoS_2 and C_3N_4 , values with asterisk were taken from the literature.⁶⁴

Overall, the UV-vis DRS, XPS and UPS spectra suggest that the composite materials behave as mechanical mixtures of individual MoS_2 and C_3N_4 , with unchanged optical band gaps and VB positions. There is no doubt that formation of heterojunction and transfer of electrons is possible in these systems and a contact between two phases is obviously important for optimal PHER performance. However, in our case the collaboration between MoS_2 and C_3N_4 seems to be mostly chemical (probably MoS_2 promotes recombination of H^* species), as it happens in many bifunctional heterogeneous catalysts. In the same lines, earlier we demonstrated for a relevant MoS_2-TiO_2 system, that the presence of an intimate contact and of an extended interface between the semiconductor and co-catalyst is not mandatory for optimal PHER catalytic performance in a liquid slurry. Thus, a combination of separated MoS_2 and TiO_2 particles in liquid methanol turned out to be more active than supported MoS_2/TiO_2 with highly dispersed and strongly interacting MoS_2 nanoslabs.²⁹ The case seems to be very similar for the $MoS_2-C_3N_4$ systems under study, containing an agglomerated MoS_2 co-catalyst.

The theoretical works that predict strong electronic modifications in the $MoS_2-C_3N_4$ materials, consider the models with extended 2D interfaces of atomically close C_3N_4 and MoS_2 slabs. In our materials the MoS_2 phase is considerably agglomerated and localized. There are no extended $MoS_2-C_3N_4$ interfaces in the major part of the sample. The increased catalytic activity was explained by harvesting of generated H^* species and their recombination on MoS_2 . A drop of activity observed at higher sulfide loading can be explained by simultaneous action of MoS_2 as a charge carriers recombination sink, as discussed in detail in Ref. ²⁹.

Conclusions

In this paper we have synthesized by a facile one-pot synthesis route a series of MoS₂-C₃N₄ composite materials. The solids proved to be active catalysts in the HDS of thiophene and photocatalytic hydrogen production. Their good HDS catalytic properties were attributed to favorable properties of C₃N₄ as a support for the active sulfide phase. The photocatalytic activity of the best MoS₂-C₃N₄ was about 30 times higher than for bare C₃N₄.

Using physical characterizations, we observed that addition of molybdenum influences the properties of carbon nitride on the preparation step: molybdenum induces structural disorder and impacts the chemical composition of carbon nitride, leading to the modification of C/N ratio and to the incorporation of considerable amounts of oxygen into the structure. According to TEM and XAS studies, molybdenum is present essentially as well-formed nanoscopic MoS₂ slabs in the whole range of loadings studied, from 0.3 to 9 wt.%.

Combining the valence band XPS, UPS and UV-vis DRS characterizations, we have constructed the band alignment diagram. Whatever the assumptions made in the spectra interpretation, the band alignment is staggered with the VB zone of molybdenum sulfide above that of carbon nitride. Moreover, we demonstrated addition of MoS₂ does not lead to modification of the C₃N₄ band gap and the positions of the CB and VB are not perturbed. Therefore, the observed increase of the PHER activity due to MoS₂ addition is attributed to its action as a chemical co-catalyst, facilitating associative desorption of hydrogen.

Acknowledgements

This work was supported by a public grant overseen by the French National Research Agency (ANR) as a part of the “Investissements d’Avenir” (ref: ANR-10-EQPX-45) provided for the building of the ROCK beamline.

References

-
- ¹ Inagaki, M.; Tsumura, T.; Kinumoto, T.; Toyoda, M. Graphitic Carbon Nitrides (g-C₃N₄) with Comparative Discussion to Carbon Materials. *Carbon* 2019, 141, 580–607.
 - ² Thomas, A.; Fischer, A.; Goettmann, F.; Antonietti, M.; Müller, J.-O.; Schlögl, R.; Carlsson, J. M. Graphitic Carbon Nitride Materials: Variation of Structure and Morphology and Their Use as Metal-Free Catalysts. *J. Mater. Chem.* 2008, 18 (41), 4893–4908.
 - ³ Goettmann, F.; Fischer, A.; Antonietti, M.; Thomas, A. Metal-Free Catalysis of Sustainable Friedel–Crafts Reactions: Direct Activation of Benzene by Carbon Nitrides to Avoid the Use of Metal Chlorides and Halogenated Compounds. *Chem. Commun.* 2006, No. 43, 4530–4532.

- ⁴ Chen, Z.; Mitchell, S.; Vorobyeva, E.; Leary, R. K.; Hauert, R.; Furnival, T.; Ramasse, Q. M.; Thomas, J. M.; Midgley, P. A.; Dontsova, D.; Antonietti, M.; Pogodin, S.; López, N.; Pérez-Ramírez, J. Stabilization of Single Metal Atoms on Graphitic Carbon Nitride. *Adv. Funct. Mater.* 2017, 27 (8), 1605785.
- ⁵ Zhang, C.; Qin, D.; Zhou, Y.; Qin, F.; Wang, H.; Wang, W.; Yang, Y.; Zeng, G. Dual Optimization Approach to Mo Single Atom Dispersed G-C₃N₄ Photocatalyst: Morphology and Defect Evolution. *Appl. Catal. B: Environ.* 2022, 303, 120904.
- ⁶ Fischer, A.; Müller, J. O.; Antonietti, M.; Thomas, A. Synthesis of Ternary Metal Nitride Nanoparticles Using Mesoporous Carbon Nitride as Reactive Template. *ACS Nano* 2008, 2 (12), 2489–2496.
- ⁷ Ryaboshapka, D.; Afanasiev, P. Carbon Nitride Used as a Reactive Template to Prepare Mesoporous Molybdenum Sulfide and Nitride. *RSC Adv.* 2021, 11 (35), 21678–21684.
- ⁸ Dang, V. D.; Adorna, J.; Annadurai, T.; Bui, T. A. N.; Tran, H. L.; Lin, L.-Y.; Doong, R.-A. Indirect Z-Scheme Nitrogen-Doped Carbon Dot Decorated Bi₂MoO₆/g-C₃N₄ Photocatalyst for Enhanced Visible-Light-Driven Degradation of Ciprofloxacin. *Chem. Eng. J.* 2021, 422, 130103.
- ⁹ Arumugam, M.; Tahir, M.; Praserthdam, P. Effect of Nonmetals (B, O, P, and S) Doped with Porous g-C₃N₄ for Improved Electron Transfer towards Photocatalytic CO₂ Reduction with Water into CH₄. *Chemosphere* 2022, 286, 131765.
- ¹⁰ Wang, X.; Maeda, K.; Thomas, A.; Takanabe, K.; Xin, G.; Carlsson, J. M.; Domen, K.; Antonietti, M. A Metal-Free Polymeric Photocatalyst for Hydrogen Production from Water under Visible Light. *Nature Mater* 2009, 8 (1), 76–80.
- ¹¹ Ong, W.-J., Tan, L.-L., Ng, Y. H., Yong, S.-T., & Chai, S.-P. (2016). Graphitic Carbon Nitride (g-C₃N₄)-Based Photocatalysts for Artificial Photosynthesis and Environmental Remediation: Are We a Step Closer To Achieving Sustainability? *Chem. Rev.*, 116 (12), 7159–7329.
- ¹² Qi, K.; Liu, S.; Zada, A. Graphitic Carbon Nitride, a Polymer Photocatalyst. *J. Taiwan Inst. Chem. Eng.* 2020, 109, 111–123.
- ¹³ Wang, L.; Wang, K.; He, T.; Zhao, Y.; Song, H.; Wang, H. Graphitic Carbon Nitride-Based Photocatalytic Materials: Preparation Strategy and Application. *ACS Sustain. Chem. Eng.* 2020, 8 (43), 16048–16085.
- ¹⁴ Niu, P.; Dai, J.; Zhi, X.; Xia, Z.; Wang, S.; Li, L. Photocatalytic Overall Water Splitting by Graphitic Carbon Nitride. *InfoMat* 2021, 3 (9), 931–961.
- ¹⁵ Zhao, H.; Dong, Y.; Jiang, P.; Miao, H.; Wang, G.; Zhang, J. In Situ Light-Assisted Preparation of MoS₂ on Graphitic C₃N₄ Nanosheets for Enhanced Photocatalytic H₂ Production from Water. *J. Mater. Chem. A* 2015, 3 (14), 7375–7381.
- ¹⁶ Saha, D.; Gismondi, P.; Kolasinski, K. W.; Shumlas, S. L.; Rangan, S.; Eslami, B.; McConnell, A.; Bui, T.; Cunfer, K. Fabrication of Electrospun Nanofiber Composite of G-C₃N₄ and Au Nanoparticles as Plasmonic Photocatalyst. *Surf. Interfaces* 2021, 26, 101367.
- ¹⁷ Raha, S.; Ahmaruzzaman, M. Facile Fabrication of G-C₃N₄ Supported Fe₃O₄ Nanoparticles/ZnO Nanorods: A Superlative Visible Light Responsive Architecture for Express Degradation of Pantoprazole. *Chem. Eng. J.* 2020, 387, 123766..
- ¹⁸ Vattikuti, S. V. P.; Byon, C. Hydrothermally Synthesized Ternary Heterostructured MoS₂/Al₂O₃/g-C₃N₄ Photocatalyst. *Mater. Res. Bull.* 2017, 96, 233–245.
- ¹⁹ Ismael, M. A Review on Graphitic Carbon Nitride (g-C₃N₄) Based Nanocomposites: Synthesis, Categories, and Their Application in Photocatalysis. *J. Alloys Compd.* 2020, 846, 156446.
- ²⁰ Zheng, D.; Zhang, G.; Hou, Y.; Wang, X. Layering MoS₂ on Soft Hollow G-C₃N₄ Nanostructures for Photocatalytic Hydrogen Evolution. *Appl. Catal. A: Gen.* 2016, 521, 2–8.
- ²¹ Han, B.; Hu, Y. H. MoS₂ as a co-catalyst for photocatalytic hydrogen production from water. *Energy Sci. Eng.* 2016, 4(5), 285–304.
- ²² Díaz de León, J.; Ramesh Kumar, C.; Antúnez-García, J.; Fuentes-Moyado, S. Recent Insights in Transition Metal Sulfide Hydrodesulfurization Catalysts for the Production of Ultra Low Sulfur Diesel: A Short Review. *Catalysts* 2019, 9 (1), 87.
- ²³ Duraisamy, S.; Ganguly, A.; Sharma, P. K.; Benson, J.; Davis, J.; Papakonstantinou, P. One-Step Hydrothermal Synthesis of Phase-Engineered MoS₂/MoO₃ Electrocatalysts for Hydrogen Evolution Reaction. *ACS Appl. Nano Mater.* 2021, 4 (3), 2642–2656.
- ²⁴ Hou, Y.; Laursen, A. B.; Zhang, J.; Zhang, G.; Zhu, Y.; Wang, X.; Dahl, S.; Chorkendorff, I. Layered Nanojunctions for Hydrogen-Evolution Catalysis. *Angew. Chem. Int. Ed.* 2013, 52 (13), 3621–3625.
- ²⁵ Yuan, H.; Fang, F.; Dong, J.; Xia, W.; Zeng, X.; Shangguan, W. Enhanced Photocatalytic Hydrogen Production Based on Laminated MoS₂/g-C₃N₄ Photocatalysts. *Colloids Surf. A: Physicochem. Eng. Asp.* 2022, 641, 128575.

- ²⁶ Cao, Y.; Gao, Q.; Li, Q.; Jing, X.; Wang, S.; Wang, W. Synthesis of 3D Porous MoS₂/g-C₃N₄ Heterojunction as a High Efficiency Photocatalyst for Boosting H₂ Evolution Activity. *RSC Adv.* 2017, 7 (65), 40727–40733.
- ²⁷ Rapti, I.; Bairamis, F.; Konstantinou, I. G-C₃N₄/MoS₂ Heterojunction for Photocatalytic Removal of Phenol and Cr(VI). *Photochem* 2021, 1 (3), 358–370.
- ²⁸ Afanasiev, P. Calculation of MoS₂ Slabs Morphology Descriptors from Transmission Electron Microscopy Data Revisited. Case Study of the Influence of Citric Acid and Treatment Conditions on the Properties of MoS₂/Al₂O₃. *Appl. Catal. A: Gen.* 2017, 529, 10–19.
- ²⁹ Afanasiev, P. MoS₂ “Inorganic Fullerenes” Combined with TiO₂ in Water-Methanol Suspensions: Highly Active Hydrogen Production Photo Catalysts Operating via Transfer of Accumulated Electrons. *Int. J. Hydrog. Energy* 2020, 45 (29), 14696–14712.
- ³⁰ Ankudinov, A. L.; Ravel, B.; Rehr, J. J.; Conradson, S. D. Real-Space Multiple-Scattering Calculation and Interpretation of x-Ray-Absorption near-Edge Structure. *Phys. Rev. B* 1998, 58 (12), 7565–7576.
- ³¹ Klementev, K. V. Extraction of the Fine Structure from X-Ray Absorption Spectra. *J. Phys. D: Appl. Phys.* 2000, 34 (2), 209–217.
- ³² Maheu, C.; Cardenas, L.; Puzenat, E.; Afanasiev, P.; Geantet, C. UPS and UV Spectroscopies Combined to Position the Energy Levels of TiO₂ Anatase and Rutile Nanopowders. *Phys. Chem. Chem. Phys.* 2018, 20 (40), 25629–25637.
- ³³ Zhao, Y.; Wei, R.; Feng, X.; Sun, L.; Liu, P.; Su, Y.; Shi, L. Dual-Mode Luminescent Nanopaper Based on Ultrathin g-C₃N₄ Nanosheets Grafted with Rare-Earth Upconversion Nanoparticles. *ACS Appl. Mater. Interfaces* 2016, 8 (33), 21555–21562.
- ³⁴ Chen, X.; Kuo, D.-H.; Lu, D. Nanonization of G-C₃N₄ with the Assistance of Activated Carbon for Improved Visible Light Photocatalysis. *RSC Adv.* 2016, 6 (71), 66814–66821.
- ³⁵ Akple, M. S.; Low, J.; Wageh, S.; Al-Ghamdi, Ahmed. A.; Yu, J.; Zhang, J. Enhanced Visible Light Photocatalytic H₂-Production of g-C₃N₄/WS₂ Composite Heterostructures. *Appl. Surf. Sci.* 2015, 358, 196–203.
- ³⁶ Shi, S.; Sun, Z.; Hu, Y. H. Synthesis, Stabilization and Applications of 2-Dimensional 1T Metallic MoS₂. *J. Mater. Chem. A* 2018, 6 (47), 23932–23977.
- ³⁷ Wang, D.; Su, B.; Jiang, Y.; Li, L.; Ng, B. K.; Wu, Z.; Liu, F. Polytype 1T/2H MoS₂ Heterostructures for Efficient Photoelectrocatalytic Hydrogen Evolution. *Chem. Eng. J.* 2017, 330, 102–108.
- ³⁸ Palencia-Ruiz, S.; Uzio, D.; Legens, C.; Laurenti, D.; Afanasiev, P. Stability and Catalytic Properties of 1T-MoS₂ Obtained via Solvothermal Synthesis. *Appl. Catal. A: Gen.* 2021, 626, 118355.
- ³⁹ Pap, G.; Bertóti, I.; Szörényi, T.; Heszler, P. The Chemical Structure of Carbon Nitride Films Fabricated by Pulsed Plasma-Assisted Chemical Vapor Deposition. *Surf. Coat. Technol.* 2004, 180-181, 271–274.
- ⁴⁰ Gao, D.; Liu, Y.; Liu, P.; Si, M.; Xue, D. Atomically Thin B Doped G-C₃N₄ Nanosheets: High-Temperature Ferromagnetism and Calculated Half-Metallicity. *Sci Rep* 2016, 6 (1), 35768.
- ⁴¹ Dong, L.; Chu, H.; Xu, S.; Li, Y.; Zhao, S.; Li, D. Band Structure Tuning of G-C₃N₄ via Sulfur Doping for Broadband near-Infrared Ultrafast Photonic Applications. *Nanophotonics* 2022, 11 (1), 139–151.
- ⁴² Dementjev, A. P.; de Graaf, A.; van de Sanden, M. C. M.; Maslakov, K. I.; Naumkin, A. V.; Serov, A. A. X-Ray Photoelectron Spectroscopy Reference Data for Identification of the C₃N₄ Phase in Carbon-Nitrogen Films. *Diam. Relat. Mater.* 2000, 9 (11), 1904–1907.
- ⁴³ Bremmer, G. M.; van Haandel, L.; Hensen, E. J. M.; Frenken, J. W. M.; Kooyman, P. J. The Effect of Oxidation and Resulfidation on (Ni/Co)MoS₂ Hydrodesulfurisation Catalysts. *Appl. Catal. B: Environ.* 2019, 243, 145–150.
- ⁴⁴ Zatoń, M.; Prélôt, B.; Donzel, N.; Rozière, J.; Jones, D. J. Migration of Ce and Mn Ions in PEMFC and Its Impact on PFSA Membrane Degradation. *J. Electrochem. Soc.* 2018, 165 (6), F3281–F3289.
- ⁴⁵ Afanasiev, P.; Lorentz, C. Oxidation of Nanodispersed MoS₂ in Ambient Air: The Products and the Mechanistic Steps. *J. Phys. Chem. C* 2019, 123 (12), 7486–7494.
- ⁴⁶ Capobianco, M. D.; Pattengale, B.; Neu, J.; Schmuttenmaer, C. A. Single Copper Atoms Enhance Photoconductivity in G-C₃N₄. *J. Phys. Chem. Lett.* 2020, 11 (20), 8873–8879.
- ⁴⁷ Mori, K.; Murakami, T.; Yamashita, H. Luminescent Single-Atom Eu-Coordinated Graphitic Carbon Nitride Nanosheets for Selective Sensing of Acetone and Cyclohexane. *ACS Appl. Nano Mater.* 2020, 3 (10), 10209–10217.
- ⁴⁸ Zhou, B.; Yang, B.; Waqas, M.; Xiao, K.; Zhu, C.; Wu, L. Design of a p–n Heterojunction in 0D/3D MoS₂/g-C₃N₄ Composite for Boosting the Efficient Separation of Photogenerated Carriers with Enhanced Visible-Light-Driven H₂ Evolution. *RSC Adv.* 2020, 10 (33), 19169–19177.

- ⁴⁹ Rao, S.; Su, C.; He, X.; Zhang, L.; Liu, Z.; Qin, H.; Rahman, N.; Liu, Q.; Yang, J. Engineering MoS₂ Cocatalysts as Active Sites over Porous P-Doped g-C₃N₄ Nanosheets to Enhance Photocatalytic Hydrogen Production. *physica status solidi (RRL) – Rapid Research Letters* 2021, 15 (12), 2000513.
- ⁵⁰ Yuan, Y.-J.; Shen, Z.; Wu, S.; Su, Y.; Pei, L.; Ji, Z.; Ding, M.; Bai, W.; Chen, Y.; Yu, Z.-T.; Zou, Z. Liquid Exfoliation of G-C₃N₄ Nanosheets to Construct 2D-2D MoS₂/g-C₃N₄ Photocatalyst for Enhanced Photocatalytic H₂ Production Activity. *Appl. Catal. B: Environ.* 2019, 246, 120–128.
- ⁵¹ Sun, J.; Yang, S.; Liang, Z.; Liu, X.; Qiu, P.; Cui, H.; Tian, J. Two-Dimensional/One-Dimensional Molybdenum Sulfide (MoS₂) Nanoflake/Graphitic Carbon Nitride (g-C₃N₄) Hollow Nanotube Photocatalyst for Enhanced Photocatalytic Hydrogen Production Activity. *J. Colloid Interface Sci.* 2020, 567, 300–307.
- ⁵² Maxim, F. I.; Tanasa, E.; Mitrea, B.; Diac, C.; Skala, T.; Tanase, L. C.; Ciocanea, A.; Antohe, S.; Vasile, E.; Stamatin, S. N. Structure and Stability of Carbon Nitrides: Ring Opening Induced Photoelectrochemical Degradation; arXiv:2103.16868; arXiv, 2021.
- ⁵³ Li, L.; Huang, Z.; Li, Z.; Li, H.; Wang, A. Defect-Rich Porous g-C₃N₄ Nanosheets Photocatalyst with Enhanced Photocatalytic Activity. *J Mater Sci: Mater Electron.* 2021, 32 (5), 6465–6474.
- ⁵⁴ Han, S. W.; Cha, G.-B.; Frantzeskakis, E.; Razado-Colambo, I.; Avila, J.; Park, Y. S.; Kim, D.; Hwang, J.; Kang, J. S.; Ryu, S.; Yun, W. S.; Hong, S. C.; Asensio, M. C. Band-Gap Expansion in the Surface-Localized Electronic Structure of MoS₂ (0002). *Phys. Rev. B* 2012, 86 (11), 115105.
- ⁵⁵ Wang, B.; Yang, S.; Chen, J.; Mann, C.; Bushmaker, A.; Cronin, S. B. Radiation-Induced Direct Bandgap Transition in Few-Layer MoS₂. *Appl. Phys. Lett.* 2017, 111 (13), 131101.
- ⁵⁶ Wang, R.; Wang, Y.; Mao, S.; Hao, X.; Duan, X.; Wen, Y. Different Morphology MoS₂ Over the G-C₃N₄ as a Boosted Photo-Catalyst for Pollutant Removal Under Visible-Light. *J. Inorg. Organomet. Polym.* 2021, 31 (1), 32–42.
- ⁵⁷ Lan, Z., Yu, Y., Yao, J., & Cao, Y. The band structure and photocatalytic mechanism of MoS₂-modified C₃N₄ photocatalysts with improved visible photocatalytic activity. *Mater. Res. Bull.* 2018, 102, 433–439.
- ⁵⁸ Chen, C.; Zang, J.; Wang, Q.; Li, Y. Loading SnS₂ Nanosheets Decorated with MoS₂ Nanoparticles on a Flake-Shaped g-C₃N₄ Network for Enhanced Photocatalytic Performance. *CrystEngComm* 2021, 23 (26), 4680–4693.
- ⁵⁹ Wang, J.; Guan, Z.; Huang, J.; Li, Q.; Yang, J. Enhanced Photocatalytic Mechanism for the Hybrid G-C₃N₄/MoS₂ Nanocomposite. *J. Mater. Chem. A* 2014, 2 (21), 7960–7966.
- ⁶⁰ Ko, H.; Kim, H. S.; Ramzan, M. S.; Byeon, S.; Choi, S. H.; Kim, K. K.; Kim, Y.-H.; Kim, S. M. Atomistic Mechanisms of Seeding Promoter-Controlled Growth of Molybdenum Disulfide. *2D Mater.* 2020, 7 (1), 015013.
- ⁶¹ Lee, H.; Deshmukh, S.; Wen, J.; Costa, V. Z.; Schuder, J. S.; Sanchez, M.; Ichimura, A. S.; Pop, E.; Wang, B.; Newaz, A. K. M. Layer-Dependent Interfacial Transport and Optoelectrical Properties of MoS₂ on Ultraflat Metals. *ACS Appl. Mater. Interfaces* 2019, 11 (34), 31543–31550.
- ⁶² Seo, D.-B.; Trung, T. N.; Kim, D.-O.; Duc, D. V.; Hong, S.; Sohn, Y.; Jeong, J.-R.; Kim, E.-T. Plasmonic Ag-Decorated Few-Layer MoS₂ Nanosheets Vertically Grown on Graphene for Efficient Photoelectrochemical Water Splitting. *Nanomicro Lett.* 2020, 12, 172.
- ⁶³ Sayan, S.; Garfunkel, E.; Suzer, S. Soft X-Ray Photoemission Studies of the HfO₂/SiO₂/Si System. *Appl. Phys. Lett.* 2002, 80 (12), 2135–2137.
- ⁶⁴ Zhu, B.; Tan, H.; Fan, J.; Cheng, B.; Yu, J.; Ho, W. Tuning the Strength of Built-in Electric Field in 2D/2D g-C₃N₄/SnS₂ and g-C₃N₄/ZrS₂ S-Scheme Heterojunctions by Nonmetal Doping. *J. Materiomics* 2021, 7 (5), 988–997.